Philosophical Magazine,
Vol. 86, Nos. 17–18, 11–21 June 2006, 2529–2536

Taylor & Francis
Taylor & Francis Group

Mapping the electron–electron interaction in gas phase C_{60}

O. KIDUN and J. BERAKDAR*

Max-Planck-Institute of Microstructure Physics, Weinberg 2,
06120 Halle, Germany

(*Received 14 February 2005; in final form 2 May 2005*)

We present a theory for studying the details of the screened electron–electron interaction in fullerenes by means of the coincident electron emission upon charged particle impact. The cross sections for this process are expressed in terms of the screened electron–electron interaction and evaluated within the random-phase approximation. We performed full quantum mechanical calculations for the cross sections and obtained fair agreement with available experiments. Furthermore, we present theoretical angular and energy-resolved cross sections to underline the wealth of information that can be gained by future experiments.

1. Introduction

A variety of physical properties of electronic materials are governed by the cooperative behaviour of electrons. Prominent examples are the emergence of Wannier excitons in wide-band semiconductors. In narrow-band materials, e.g. in 3d transition metal oxides or in rare earths, Coulomb interactions may result in insulating (magnetic) ground states. The role of electronic correlation is ubiquitous in that it also determines some important features of molecular and polymeric materials. For example, C_{60} doped with alkali metals acquires superconductive features, hence, calling for an investigation of the role of the electron–electron (e–e) interaction in this molecular material [1, 2]. A theoretical study of the nature of the e–e interaction in solid (ordered) phase C_{60} concluded that the screened on-site molecular Coulomb integral is $\sim$2.1 eV [3]. In addition to this energetic feature, an important concept for inspecting the e–e interaction is screening. Screening effects can be quantified by the dielectric function [4]. Experiments reported by Hansen *et al*. [5] give an estimate of 4.6 for the value of C_{60} macroscopic dielectric function, whereas Ren *et al*. [6] estimates this value to be 3.6. These numbers mean a weak screening in solid C_{60}; however, they do not offer an insight into the angular and the energy dependence of screening of the e–e interaction, in particular, as far as gas-phase fullerenes are concerned. It is the purpose of this work to present a new spectroscopic tool to shed light on the various facets of the electron–electron

*Corresponding author. Email: jber@mpi-halle.de

Philosophical Magazine
ISSN 1478–6435 print/ISSN 1478–6443 online
http://www.tandf.co.uk/journals
DOI: 10.1080/14786430500333307

interaction in matter. The method relies on disturbing the system by charged particles. The system may then react by ejecting one or more electrons. As shown below, resolving the energies and momenta of the final-state particles offers the possibility of accessing information on the details of the electron–electron interaction.

The paper is organized as follows. In section 2, we present a general framework for the treatment of screening in collision processes. In section 3, the theory is applied to electron and proton scattering from fullerenes C_{60}. Section 4 contains conclusions and final remarks. Unless otherwise specified, atomic units (a.u.) $\hbar = e = m_e = 1$ are used throughout.

2. General considerations

A schematic view of the process under study is depicted in figure 1. A target prepared in the quantum state $|\phi_\nu\rangle$ is perturbed by a projectile that has a specified quantum state $|\mathbf{k}_0\rangle$, where $\mathbf{k}_0$ is the momentum of the impinging particle. In the final state, two electrons emerge with the asymptotic momenta $\mathbf{k}_1$ and $\mathbf{k}_2$. In electron energy loss spectroscopy (EELS), only one electron [7] is measured. One usually assumes that this electron is the projectile electron, which has suffered some amount of energy and momentum loss. As well-established, the EELS cross section is then related to the imaginary part of the dielectric function. The difference between EELS and the process shown in figure 1 is inferred from the energy balance: if the energy lost by the projectile is not sufficient to overcome the work function, the electron emission channel is closed, i.e. the process in figure 1 is not possible and one measures an EELS signal associated with neutral excitations, such as plasmon generation. On the other hand, the energy loss of the projectile may well be so high as to excite a target electronic state into the vacuum. In such a case, the process in figure 1 contributes to the EELS cross section. However, what is then measured in EELS provides only integral information. More details are obtained by detecting both excited states $\mathbf{k}_1$ and $\mathbf{k}_2$ at the same time. Another possibility of tracing the occurrence of the process in figure 1 is to detect the charge

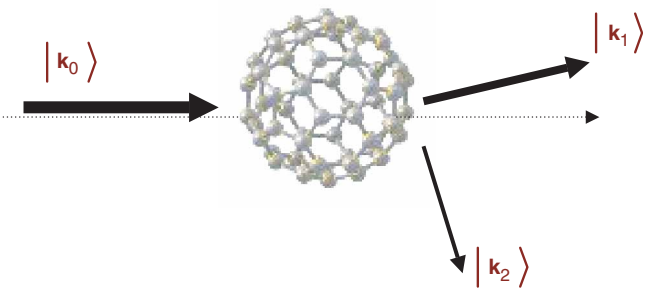

Figure 1. Schematic drawing of the emission process of an electron with a wave vector $\mathbf{k}_2$ for C_{60} upon the impact of a charged particle with the wave vector $\mathbf{k}_0$. The momentum of the scattered particle is $\mathbf{k}_1$. The z-axis is chosen as the direction of the incoming particle $\mathbf{k}_0$.

state of the target in the final channel. This possibility allows measuring, for example, the integrated (total) cross sections, while still singling out the electron emission channel.

The transition matrix elements $\mathsf{T}(\mathbf{k}_1\mathbf{k}_2,\phi_\nu\mathbf{k}_0)$ of the electron emission process (figure 1) can be evaluated in first-order perturbation theory in the (unknown) electron–electron interaction U_{eff}, which amounts to using the so-called random-phase approximation (RPA) (in the case of a projectile electron, one has also to account for exchange effects; in such a case, we use RPAE, i.e. RPA with exchange). *A posteriori*, we will find that this approach is justified for moderately large systems, such as C_{60}, due to the fact that screening is substantial. Within RPAE, the matrix elements $\mathsf{T}(\mathbf{k}_1\mathbf{k}_2,\phi_\nu\mathbf{k}_0)$ are given by the equation [8]:

$$\begin{aligned}\mathsf{T}(\mathbf{k}_1\mathbf{k}_2,\phi_\nu\mathbf{k}_0) &= \langle \mathbf{k}_1\mathbf{k}_2 | U_{\mathrm{eff}} | \phi_\nu\mathbf{k}_0\rangle \\ &= \langle \mathbf{k}_1\mathbf{k}_2 | U | \phi_\nu\mathbf{k}_0\rangle + \sum_{\substack{\varepsilon_{\mathrm{h}}>\mu \\ \varepsilon_{\mathrm{p}}\le\mu}} \left(\frac{\langle \varphi_{\mathrm{p}}\mathbf{k}_2 | U_{\mathrm{eff}} | \phi_\nu\varphi_{\mathrm{h}}\rangle\langle \varphi_{\mathrm{h}}\mathbf{k}_1 | U | \mathbf{k}_0\varphi_{\mathrm{p}}\rangle}{\varepsilon_0 - (\varepsilon_{\mathrm{p}} - \varepsilon_{\mathrm{h}} - \mathrm{i}\delta)} \right. \\ &\quad \left. - \frac{\langle \varphi_{\mathrm{h}}\mathbf{k}_2 | U_{\mathrm{eff}} | \phi_\nu\varphi_{\mathrm{p}}\rangle\langle \varphi_{\mathrm{p}}\mathbf{k}_1 | U | \mathbf{k}_0\varphi_{\mathrm{h}}\rangle}{\varepsilon_0 + (\varepsilon_{\mathrm{p}} - \varepsilon_{\mathrm{h}} - \mathrm{i}\delta)} \right). \end{aligned} \tag{1}$$

This integral equation has to be solved (numerically) to obtain the effective interaction U_{eff} between the test particle (the projectile) and the target electronic state ϕ_ν. In equation (1), ε_0 is the energy of the incoming particle and $\varepsilon_{\mathrm{p/h}}$ are the energies of, respectively, the particle and the hole states φ_{p} and φ_{h}, and U is the naked Coulomb interaction. The sum in equation (1) runs over all particle and hole states up to the Fermi level μ. To make the connection between equation (1) and the linear response theory clearer, we write equation (1) formally as $U_{\mathrm{eff}} = U + U_{\mathrm{eff}}\,\Pi\,U$, where Π is the polarization propagator. This relation can be rewritten as $U_{\mathrm{eff}} = U/\varepsilon$, where $\varepsilon = 1 - \Pi U$ is the dielectric function.

Currently, only integrated cross sections for the process of figure 1 have been measured [9, 10], i.e. these experiments do not resolve the momenta and the spins $\sigma_{1,2}$ of the particles in the final state, but they do resolve the projectile energy and the target charge states. To compare with these experiments we have to evaluate the total cross section W as:

$$W(\varepsilon_0) = \frac{(2\pi)^2}{k_0} \int d^3\mathbf{k_1}\, d^3\mathbf{k_2} \sum_{\sigma_1\sigma_2\phi_\nu} \left| \langle \mathbf{k}_{1,\sigma_1}\mathbf{k}_{2,\sigma_2} | U_{\mathrm{eff}} | \phi_\nu\mathbf{k_0}\rangle \right|^2. \tag{2}$$

From equations (1) and (2) it is clear that the calculations of the matrix elements and the cross sections entail knowledge of the electronic particle and hole states of the target in the ground state (before the collision), as well as its scattering states. These states have to be calculated independently for each individual system and, with this knowledge, we then solve the integral equation (1) to determine the dressed particle–particle interaction U_{eff}. So, even though U has a universal structure independent of the system, U_{eff} is in general strongly system dependent. It is this dependency that can be revealed by the process depicted in figure 1.

3. Numerical results

As an example, we calculate the total cross section (2) for the ionization of the valence band electrons in C_{60} by numerically solving equation (1) and then performing a numerical Monte Carlo integration to evaluate the six-dimensional integral in equation (2).

The single hole and particle states of the fullerene are derived from self-consistent Hartree–Fock calculations; thus, we incorporate (for the ground-state calculations) the mean-field part of the electron–electron interactions and exact exchange effects. Both bound and scattering wave functions are calculated simultaneously using the non-local variable phase method [11–13], which proved indispensable for the numerical realization. For the fullerene shell, we employ a model potential that incorporates correctly the experimentally determined radius of C_{60}, the distance between the neighbouring carbon nuclei (C–C bond length) and the affinity energy of the electron to the singly charged fullerene. This model has been used previously [14, 15]; however, the calculation was made on the basis of density functional theory within the local-density approximation and without performing the RPAE loop. The resulting potential, formed by the carbon ions and the localized core electrons, is a shifted potential well: $V_{\mathrm{ion}}(r) = V_0$ for $R - \delta < r < R$, and $V_{\mathrm{ion}}(r) = 0$ elsewhere. Here, $R \sim 6.65$ a.u. is the radius of the fullerene. The average C–C bond length is the thickness of the well $\delta \sim 2.69$ a.u. The depth V_0 is determined such that the experimental value of the first ionization potential of C_{60} is 7.6 eV and the number of valence electrons is 240.

To illustrate the structure of the potential experienced by the valence electrons, we plot in figure 2 the calculated local part only of the self-consistent single-particle potential V_{SC} for a valence band electron with a zero angular momentum. From this figure, it is evident that the mean-field part of the electron–electron interaction and the local part of the exchange interaction result in a marked modification of the external potential V_{ion} (in fact the potential V_{SC} is non-local and contains, in general, a centrifugal term).

The numerical results obtained upon performing the calculations required by equation (2) are shown in figure 3 and compared to other calculations and available experiments. Two important observations can be made here: the effect of screening is substantial in the low-frequency regime, even for relatively small systems such as C_{60}. In the high-frequency regime, we see no effect of screening because the characteristic frequency of the retarded response of the target is far from the perturbation frequency.

These two observations justify our use of the first-order perturbation theory in the projectile electron–valence electron interaction (in the high-energy regime, this approach is valid anyway). Figure 3 shows that electron emission is suppressed by the screening of the perturbation caused by the incoming particles. The delocalized valence electrons cooperatively rearrange so as to reduce, at the C_{60} cage surface, the external electric field. This is not achievable for high-projectile energies and small impact parameter and, hence, screening has no sizable effect in the high-energy range in figure 3. This interpretation follows also from equation (1): in the simplest approximation, the cross section (2) is proportional to the form factor of $U_{\mathrm{eff}}(q)$, where $\mathbf{q}=\mathbf{k}_0—\mathbf{k}_1$ is the momentum transfer vector. From the theory of homogenous

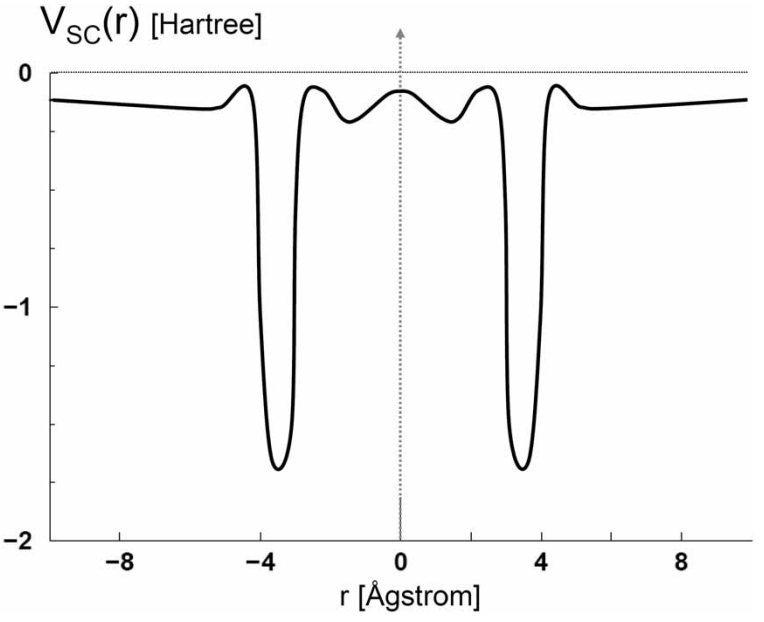

Figure 2. Calculated local part of the self-consistent single-particle potential V_{SC}(r) for a valence band electron in C_{60} that has a vanishing angular momentum. V_{SC} is plotted as a function of the radial distance r (in Å) measured from the cage centre of C_{60}.

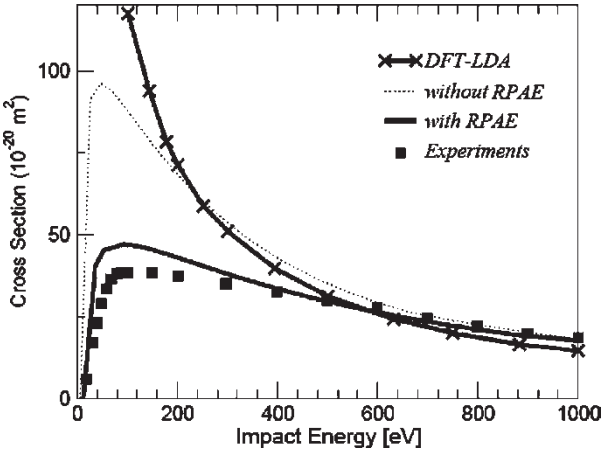

Figure 3. Absolute total cross section for the removal of one electron from C_{60} following the impact of an electron with the energy displayed on the axis. The experimental data (filled squares) are from [9, 10]. The solid curve with crosses is the result of density functional theory calculations done within local-density approximation and reported in [14]. The dotted curve shows the present theory without RPAE. Theoretical results based on RPAE are shown by the solid curve.

electron gas, we know that in the long-wave length limit $U_{\text{eff}}(q) \sim U_{\text{eff},TF}(q) \sim 1/(q^2+\lambda^2)$, where $1/\lambda$ is the screening length. Our calculations show indeed that the Fourier transform of the potential U_{eff} can, to some extent, be modelled by the potential $U_{\text{eff},TF}(q)$. On the other hand, from the form of $U_{\text{eff},TF}(q)$, we conclude that for a large q, i.e. close collision, $U_{\text{eff},TF}(q) \to U(q)$, where $U(q)$ is the naked Coulomb interaction, but for a small momentum transfer, i.e. distant collisions, we infer that $U_{\text{eff},TF}(q) \sim \text{constant} = 1/\lambda^2$, which indeed explains the saturation effect of the cross section observed in figure 3 as compared to the unscreened calculations.

The calculations and the experiments shown in figure 3 contain a contribution from exchange effects due to the fact that the projectile is an electron. To get an insight, both experimentally and theoretically, into the importance of these effects, one can use a test projectile particle other than electrons. Here, we employ protons. Neglecting screening, we find within our first-order theory for the projectile target interaction that there should be no difference in the ionization cross sections induced by equivelocity projectiles that have the same magnitude of charge, e.g. equal-velocity electrons and protons should lead to the same ionization cross section. Applying RPA, a difference between these two cases arises solely due to the fact that, in the case of the proton, the exchange contributions are absent.

These contributions are quite sizable as demonstrated by figure 4, where the ratio of the cross sections for proton and electron impact ionization of the valence band of C_{60} is plotted against the impact velocity of the projectile. At a velocity of approximately 10 a.u., screening effects become negligible and protons and electrons are equivalently effective in ionizing the target, as also follows from the first Born theory of ionization. At lower velocities, however, exchange effects, active in the case of a projectile electron, suppress the ionization cross sections by a factor of up to 1.5, as compared to the proton-impact ionization cross sections.

To exploit the full power of the present spectroscopic technique, one should perform angular and energy resolve coincidence measurements. Such experiments

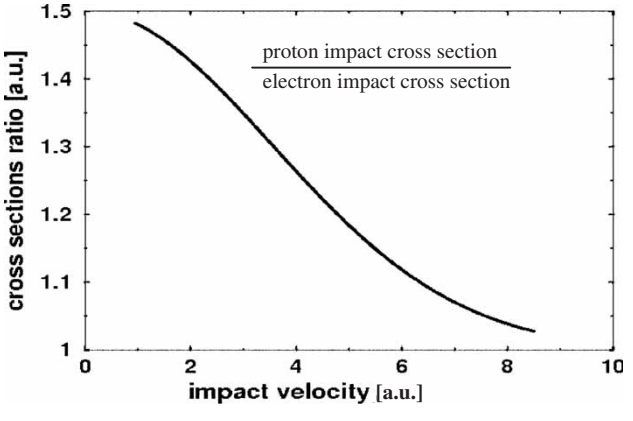

Figure 4. Ratio of absolute total ionization cross sections of the valence band of C_{60} by proton and electron impact as a function of the projectile impact velocity. The electron impact ionization cross section is shown by the solid curve in figure 3.

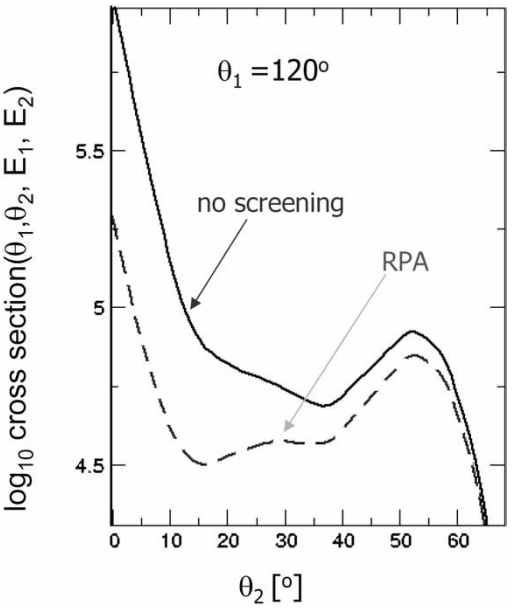

Figure 5. Angular dependence of the fully differential cross section for the emission of one electron from C_{60} with 1 eV energy following the impact of 50 eV electrons. A schematic of the scattering geometry is depicted. The scattering angle θ_1 of the scattered electron is fixed at 120°, whereas the emission angle θ_2 of the second electron is varied. Calculations with (dashed line) and without (solid line) screening are compared.

allow accessing experimentally the energy and angular dependence of the magnitude $|T|^2$ of the transition matrix elements, as given by equation (1). As is evident from equation (1), $|T|^2$ in turn contains information on the energy and angular dependence of the screened particle–particle interaction characteristic for the system under study. This kind of experiment has not been conducted yet. Typical calculations are shown in figure 5. The origin of the structures seen in the cross sections lies in the nature of U_{eff} and in the details of the electronic structure of the target. In the context of the present work, we emphasize the strong angular dependence of the electron–electron screening; different values of θ_1 in figure 5 yield different angular distributions of the cross section as a function of θ_2. To the best of our knowledge, such a detailed study of the screened electron–electron interaction in electronic material is not accessible by any other spectroscopic tool. In particular, EELS is not capable of providing such information.

5. Summary and conclusions

In summary, in this theoretical study, we envisaged the use of coincident electron emission from fullerene by charged particle impact as a tool for studying the details of the screened electron–electron interaction. We presented a formal theory to

evaluate the cross sections for this process and performed full quantum calculations that are in fair agreement with available experiments. Furthermore, we pointed out the need for further experimental investigations to separate the exchange-driven contributions to screening and to obtain full information on the angular and energy dependence of the screening of the electron–electron interaction in the valence band of fullerenes. As shown in [8], much of these findings are also valid for other nano-sized systems, such as metal clusters.

References

[1] A.F. Hebard, *et al.*, Nature **350** 600 (1991).
[2] R.W. Lof, *et al.*, Phys. Rev. Lett. **68** 3924 (1992); J. Electron. Spectrosc. Relat. Phenom. **72** 83 (1995).
[3] D.P. Joubert, J. Phys. Condens. Mat. **5** 8047 (1993).
[4] O. Gunnarsson and G. Zwicknagel, Phys. Rev. Lett. **69** 957 (1992).
[5] P.L. Hansen, *et al.*, Chem. Phys. Lett. **181** 367 (1991).
[6] S.R. Ren *et al.*, Appl. Phys. Lett. **59** 2678 (1991).
[7] H. Ibach and D.L. Mills, *Electron Energy Loss Spectroscopy and Surface Vibrations* (Academic Press, New York, 1982).
[8] O. Kidun and J. Berakdar, Phys. Rev. Lett. **87** 263401 (2001).
[9] S. Matt, *et al.*, J. Chem. Phys. **105** 1880 (1996).
[10] V. Foltin, *et al.*, Chem. Phys. Lett. **289** 181 (1998).
[11] F. Calogero, Nuovo Cimento **33** 352 (1964).
[12] V. Babikov, *Method of the Phase Functions in Quantum Mechanics* (Nauka, Moscow, 1971).
[13] O. Kidun, N. Fominykh and J. Berakdar, J. Phys. A **35** 9413 (2002).
[14] S. Keller and E. Engel, Chem. Phys. Lett. **299** 165 (1999); S. Keller, Eur. Phys. J. D **13** 51 (2001).
[15] M. Brack, Rev. Mod. Phys. **65** 677 (1993).